
KTH Engineering Sciences

# Strain Gradient Plasticity Modelling of Precipitation Strengthening

Mohammadali Asgharzadeh

Doctoral thesis no. 57, 2018
KTH School of Engineering Sciences
Royal Institute of Technology
SE-100 44 Stockholm Sweden

TRITA-SCI-FOU 2018:57
ISBN: 978-91-7873-072-8

Akademisk avhandling som med tillstånd av Kungliga Tekniska Högskolan i Stockholm framlägges till offentlig granskning för avläggande av teknisk doktorsexamen onsdagen den 13 februari kl. 10:00 i Kollegiesalen, hörsal 78, Kungliga Tekniska Högskolan, Brinellvägen 8, Stockholm.

To all great teachers of mine

“If we knew what we were doing, it wouldn’t be called research!”

– Albert Einstein

“The struggle itself is enough to fill a man's heart. One must imagine Sisyphus happy.”

– *The Myth of Sisyphus,* Albert Camus

# Abstract

The introduction of particles and precipitates into a matrix material results in strengthening effects. The two main mechanisms involved in this matter are referred to as Orowan and shearing. To numerically study this phenomenon is the motivation to the research done, which is presented here in this thesis. The heterogeneous microscale state of deformation in such materials brings in size scale effects into the picture. A strain gradient plasticity (SGP) theory is used to include effects of small scale plasticity. In addition, a new interface formulation is proposed which accounts for the particle-matrix interactions. By changing a key parameter, this interface model can mimic the level of coherency of particles, and hence is useful in studying different material systems.

The governing equations and formulations are then implemented into an in-house SGP FEM program. The program is equipped with axi-symmetric and three-dimensional modelling capabilities. Different distributions of particles are considered, from which proper representative volume elements (RVEs) are constructed. These RVEs are then analyzed under different loadings, and homogenization methods are utilized to evaluate macroscopic response of the material. A quantity of interest is the increase in yield stress of material due to presence of particles and precipitates. Comprehensive parametric studies are carried out to study the effects of different parameters on the strengthening. A closed-form solution is obtained, which suggests the strengthening increases by increasing the surface area of particles per unit volume of material.

The work done is presented in four appended papers. *Paper A* uses an axi-symmetric model to set the theoretical basis for the rest of the papers. Effects of different key parameters on the strengthening are studied and presented in this paper. Since the axi-symmetric model is numerically cheap, an extensive amount of analyses are carried out. *Paper B* is about the expansion of the theory introduced in the first paper into 3D space. The micromechanical model is composed of a cuboid RVE with eight different particles, one at each corner. The inclusion of more than one particle is a key parameter in studying the effects of size distribution.

The idea of having the most general micromechanical model is the theme of *Paper C*. Here, a completely random distribution of particles in 3D space is taken into account. In addition, the results of all carried out analyses are tested against experimental results from different material systems. Last paper, *Paper D*, summarizes a successful effort to include Shearing mechanism in the micromechanical model. The RVE is equipped with an embedded slip plane, and yet has the features introduced in previous papers. Hence, it has the ability to cover both strengthening mechanisms observed in precipitated materials.

# Sammanfattning

Partiklar och utskiljningar i ett material ger materialet ökad styrka. Orsakerna till denna effekt är relaterade till två mekanismer som brukar benämnas Orowan och skjuvning. Att utveckla en kontinuummekanist baserad metod för att studera denna effekt numeriskt har varit motivationen till forskningen utförd i denna avhandling. Det heterogena deformationstillståndet på mikroskala i dessa material leder till att en längdskala kommer in i bilden, och för att inkludera effekter av plastisk deformation på denna skala har en plastisk töjningsgradientteori använts. Dessutom, är en ny modell för gränsskiktet mellan en partikel och omkringliggande material föreslagen för att inkludera denna växelverkan. Partiklars koherens kontrolleras av en modellparameter, vilket innebär att modellen kan användas till att studera olika materialsystem.

Modellen är implementerad i ett FEM-program för analys av två- och tre-dimensionella problem. Representativa material volymer (RMV) har konstruerats genom att beakta ett antal olika relevanta partikelfördelningar. Dessa RMV har sedan analyserats för olika spänningstillstånd och materialets makroskopiska respons har erhållits genom homogenisering. Av speciellt intresse i dessa analyser är hur ökningen av sträckgräns beror av egenskaperna för de partiklarna som ingår i en RMV, och omfattande parameterstudier har utförts för att kartlägga detta. Baserat på resultaten från dessa studier har ett slutet uttryck för ökningen av sträckgräns som funktion av ett fåtal relevanta modellparametrar formulerats, vilket är ett centralt resultat. Sträckgränsökningen är proportionell mot den totala ytan av partiklarna i en RMV, där proportionalitetskonstanten bestäms av gränsskiktets egenskaper.

Det utförda arbetet är presenterat i fyra bilagda artiklar. I artikel A används en axisymmetrisk modell för att undersöka den föreslagna modellen egenskaper, vilket också lagt den teoretiska grunden för de resterande artiklarna. Identifiering av primära parametrar och dess inflytande på ett materials styrka presenteras i denna artikel. Då beräkningstiden för en axisymmetrisk analys är starkt begränsad utfördes omfattande numeriska studier med denna modell. I artikel B utvidgas studien till tre dimensioner, där en RMV bestående av ett rätblock innehållande 8 periodiskt placerade partiklar av varierande storlek.

Temat för artikel C är att utveckla en helt generell RMV i tre dimensioner som innehåller en slumpartad fördelning av upp till 17 partiklar. Dessutom, jämförs modellen framgångsrikt med experimentella resultat från ett antal olika materialsystem. I sista artikeln, artikel D, utökas modelleringskonceptet med skjuvningsmekanismen genom att införa ett diskret glidplan som även innefattar partikeln. Analyserna i D belyser på ett tydligt sätt när de två mekanismerna samverkar till att ge ökad styrka åt materialet alternativt dominerar beteendet.

# Acknowledgments

There are hundreds of quotes on how insignificant money is, but as a matter of fact, every project boils down to funding, and this is why I would like to start these paragraphs by thanking both VINN Excellence Center Hero-m and Department of Solid Mechanics at KTH, whose financial support made it possible to carry out the research presented in this doctoral thesis from 2013 to 2018. Money is similar to fuel for a road trip. It is essential, but what is more important is having good vision to reach the destination and enjoy the journey, and it is through proper guidance that such a perception is created. This is what my supervisors, Prof. Jonas Faleskog and Dr. Carl Dahlberg, have done very well. I am happy I did my PhD under the supervision of two of the gifted researchers in this field, and I am thankful for that.

However, even the best technical support will not save you from feeling low on bad days and sad days, and believe me, PhD life is full of those. The code is not working, the deadline is arriving, the reviewer has rejected your article, the supervisor isn't buying what you sell, the department isn't buying what you want, the stupid printer needs repair, there are no teabags left. That is when you need the moral support of your friends, who are there to cheer you up and encourage you to continue, and you, my fellow PhD students, you were there for me all the time. I would like to take the opportunity to thank each and every one of you – Eric, Ester, Kurosh, Mahdi, Micke, and Petter, to name but a few.

And of course, who could survive hardships of life, including PhD time, without the emotional support of their beloved ones. Älskade Elin, baba Ebrahim, maman Tahereh, abji Fati, and dadash Amir, I love you guys, and I am sincerely grateful for your unconditional support throughout these years. And finally, I want to conclude these paragraphs with a note to Future Me, who is most probably the only person taking this print out of bookshelf and reading it in five years. Remember that you stayed and struggled and failed and lost hope and fought and got motivated and succeeded and repeated this loop again and again! Let those ups and downs remind you that your endurance limit is surprisingly high, so you know you will survive what is waiting for you on the roller-coaster which is life!

Stockholm, Winter 2018

# List of appended papers

**Paper A:** Strengthening effects of particle-matrix interaction analyzed by an axi-symmetric model based on strain gradient plasticity
Mohammadali Asgharzadeh and Jonas Faleskog
*Report TRITA-SCI-RAP 2018:006, Department of Solid Mechanics, School of Engineering Sciences, KTH Royal Institute of Technology, Stockholm, Sweden*
Submitted for publication

**Paper B:** A model for precipitation strengthening accounting for variations of particle size and spacing based on strain gradient plasticity in 3D
Mohammadali Asgharzadeh and Jonas Faleskog
*Report TRITA-SCI-RAP 2018:007, Department of Solid Mechanics, School of Engineering Sciences, KTH Royal Institute of Technology, Stockholm, Sweden*
Submitted for publication

**Paper C:** A 3D model for the analysis of plastic flow properties of randomly-distributed particles
Mohammadali Asgharzadeh, Carl F. O. Dahlberg and Jonas Faleskog
*Report TRITA-SCI-RAP 2018:008, Department of Solid Mechanics, School of Engineering Sciences, KTH Royal Institute of Technology, Stockholm, Sweden*
To be submitted

**Paper D:** A shearing/looping transition model for precipitation strengthening
Mohammadali Asgharzadeh and Jonas Faleskog
*Report TRITA-SCI-RAP 2018:009, Department of Solid Mechanics, School of Engineering Sciences, KTH Royal Institute of Technology, Stockholm, Sweden*
To be submitted

# Author's contribution

The author's contribution to the appended papers is as following:

*Paper A:* Principal author. Performed FEM implementation, preparation of models, execution of analyses, and compiling the manuscript. Jonas Faleskog collaborated in setting the theoretical framework and development of FEM models, contributed to the manuscript, and supervised the process.

*Paper B:* Principal author. Performed FEM implementation, preparation of models, execution of analyses, and compiling the manuscript. Jonas Faleskog collaborated in setting the theoretical framework and development of FEM models, and supervised the process.

*Paper C:* Principal author. Performed FEM implementation, preparation of models, execution of analyses, and compiling the manuscript. Carl Dahlberg supplied the random distribution of particles and its statistical features, and contributed to the manuscript. Jonas Faleskog collaborated in setting the theoretical framework and development of FEM models, and supervised the process.

*Paper D:* Principal author. Performed FEM implementation, preparation of models, execution of analyses, and compiling the manuscript. Jonas Faleskog collaborated in setting the theoretical framework and development of FEM models, and supervised the process.

# Other contributions

In addition to the appended papers, the work has resulted in the following publications and presentations:

**Study of Precipitation Hardening using SGP Theory**
Mohammadali Asgharzadeh and Jonas Faleskog
Presented at Hero-M Annual Workshop, Stockholm, 2014

**Parametric Study of Precipitation Hardening using SGP Theory**
Mohammadali Asgharzadeh and Jonas Faleskog
Presented at Svenska Mekanikdagar, Linköping, 2015

**Study the Effects of Distribution of Particle Size and Spacing on Precipitation Hardening**
Mohammadali Asgharzadeh and Jonas Faleskog
Presented at Hero-M Annual Workshop, Stockholm, 2015

**A 3D-, SGP-based Model to Study the Effects of Distribution of Particle Size and Spacing on the Plastic Flow Properties of Precipitation-hardened Materials**
Mohammadali Asgharzadeh and Jonas Faleskog
Presented at International Congress of Theoretical and Applied Mechanics (ICTAM), Montréal, 2016

**An Interface Model to Study Precipitation Strengthening**
Mohammadali Asgharzadeh and Jonas Faleskog
Presented at Hero-M Annual Workshop, Stockholm, 2016

**Continuum Analysis of Precipitation Hardening Using SGP Theory**
Mohammadali Asgharzadeh and Jonas Faleskog
Presented at International Conference on Computational Plasticity (COMPLAS), Barcelona, 2017

**Precipitation Strengthening; Shearing and Orowan Mechanisms**
Mohammadali Asgharzadeh and Jonas Faleskog
Presented at Hero-M Annual Workshop, Stockholm, 2017

**Analysis of Precipitation Hardening**
Mohammadali Asgharzadeh and Jonas Faleskog
Presented at International Engineering Science Consortium Symposium (IESC), Stockholm, 2018

# Contents

# Introduction

The macroscopic behavior of multi-phase metallic materials depends on their complex micro-structures, since size scale effects will emerge if the state of deformation at the micro scale is heterogeneous. Such micro-structures can be found in materials with fine particles and precipitates in their matrix. These particles will interact with moving dislocations –dominant carriers of plasticity– which result in a couple of strengthening mechanisms, known as precipitation (particle) strengthening.

The work of research presented in this thesis is an endeavor to study the phenomenon of precipitation strengthening. First, the following pages will give an introduction on the underlying principles of the current study. These include the physical background of the phenomenon, the theoretical framework of the analysis, the implementation of such framework into computational tools, the definition of problem and modeling, and a summary of results. Appended papers will come after, in which the details of research are comprehensively discussed.

# Physical background

Plastic deformation in metallic materials is initiated by introduction and movement of lattice imperfections in form of dislocations. Figure 1 depicts two types of dislocations, namely edge and screw dislocations. Dislocations move along specific ordered planes in the crystal, called slip planes, with the motion being driven by a stress acting along the slip plane called the resolved shear stress (RSS). Figure 2 shows an edge dislocation movement.

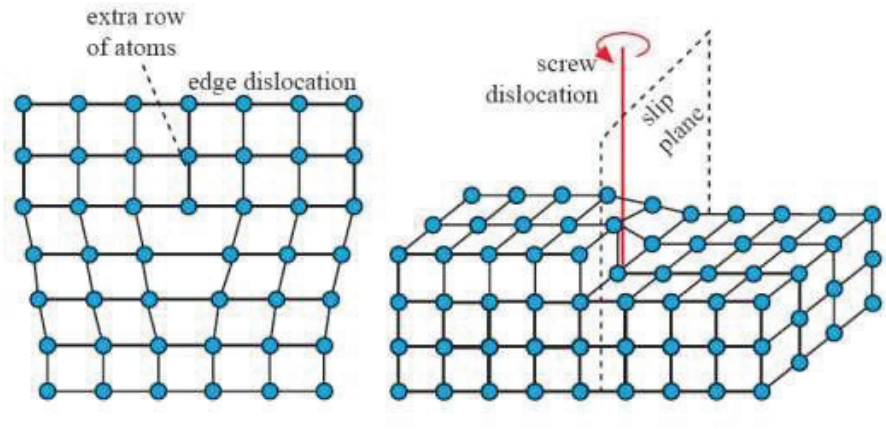


Figure 1: Edge and screw dislocations. Figure taken from McNamara (2009).

If there were no obstacles to the movement of dislocations, a material crystal would deform elastically under an applied stress. When RSS reaches its critical value on a slip plane, a dislocation would have been activated and moved according to the applied stress. After that, another slip plane would have been activated and this process would have repeated itself, resulting in a step-like surface. Finally, a material crystal would have sheared off completely. But in real material systems, a perfect slip plane rarely exists, since there are many impurities and inclusions in the material which intersect with slip planes. One notable example of these obstacles are second-phase particles.

As dislocations move, they hit the particles intersecting the slip plane. Depending on particle properties (its size, coherency, shear modulus mismatch, and volume fraction),

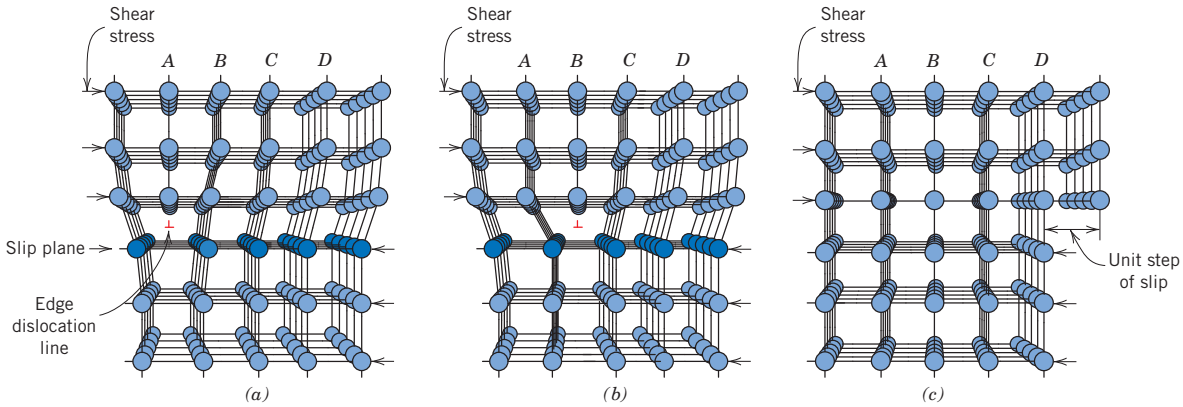


Figure 2: Movement of an edge dislocation. Figure taken from D Callister (2018).

four possible mechanisms may occur: *i)* dislocations shear (cut through) particles; *ii)* dislocations loop around particles as in the so-called Orowan mechanism; *iii)* screw dislocations cross slip; *iv)* edge dislocations climb (Jonsson (2007)). Climb mechanism only happens under high temperature creep conditions, and cross slip mechanism requires high stress levels on secondary slip systems, which makes it occur less often, as the Orowan mechanism would be invoked before reaching such high stress levels. Hence, the dominating mechanisms in presence of second-phase particles are shearing and Orowan.

**Shearing mechanism** occurs for small and coherent particles. Coherency means that the slip plane continue through the particle, so the dislocation can enter the particle and shear it. The shearing is done in the direction of Burgers vector. Coherent particles normally posses ordered structures. As a dislocation passes through the particle, this order gets broken. However, if a second dislocation follows, the order will be restored, and part of the energy lost by the first dislocation will be refunded to the second one. Hence, dislocations normally shear particles in pairs (see figure 3). Figure 4 shows a real example of particle shearing. As can be seen, dislocations have cut through particles using similar slip planes, since the cross section of particles reduce each time they are cut through, and therefore it is easier for dislocations to shear through the same slip plane. This fact makes the state of deformation highly localized (heterogeneous), which means size scale effects will play a role in material's response (see next section for further details).

**Orowan mechanism** occurs for large and incoherent particles. As particles become incoherent, dislocations cannot pass through them anymore. So, when dislocations approach impenetrable particles, they expand towards the space between particles and enclose sidewise. When two ends of dislocations meet each other, they annihilate and leave a ring of dislocation around the particles, known as Orowan loops (see figure 5). The dis-

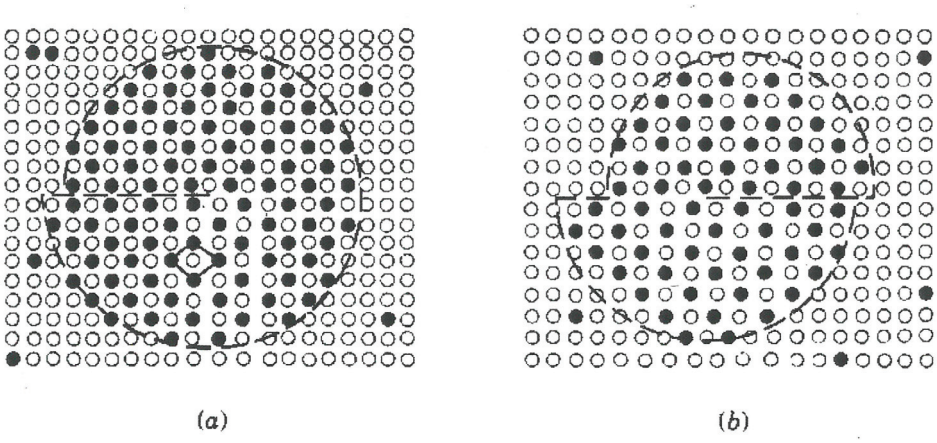


Figure 3: Shearing of a particle with ordered structure. Figure taken from Jonsson (2007).

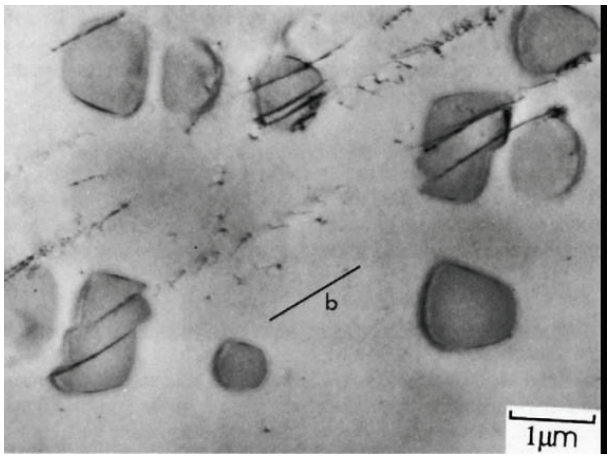


Figure 4: Shearing of $Ni_3Si$ particles in a $Ni - 6\%Si$ crystal. Figure taken from Rollett et al. (2017).

location segment left behind the particle will continue its movement. It should be noted that the area enclosed by Orowan loops has not been swept by dislocations, and hence, has not been deformed plastically. Dislocations should first bend into a minimum curvature before passing particles. As a simplified approximation, if the curvature is taken to be $L$ (the distance between two particles), the critical RSS for Orowan mechanism will be

$$\tau_{\text{Orowan}} = \frac{Gb}{L} \tag{1}$$

in which $G$ is the shear modulus and b is the magnitude of Burgers vector. Figure 6 shows a real example of Orowan mechanism. As more loops are added around particles, the looping requires higher levels of stress to occur (since the passageway between particles becomes narrower to pass), and therefore, material demonstrates hardening.

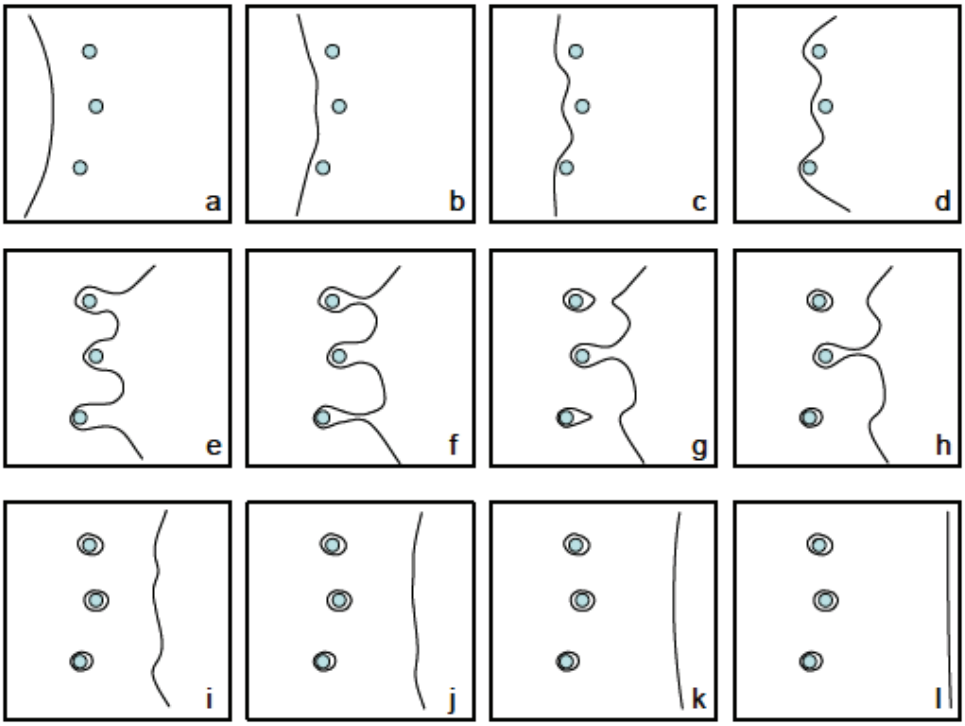


Figure 5: Schematic of Orowan mechanism. Figure taken from Jonsson (2007).

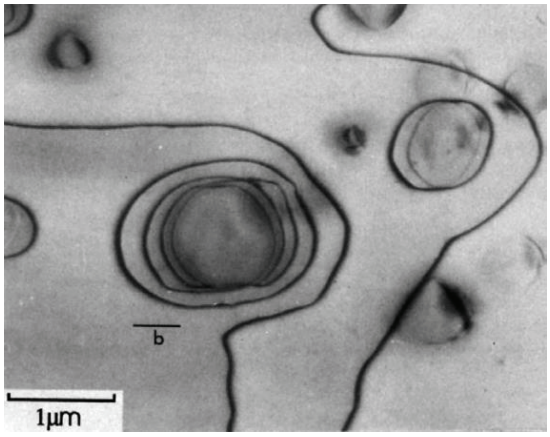


Figure 6: Orowan looping of $Ni_3Si$ particles in a $Ni - 6\%Si$ crystal. Figure taken from Rollett et al. (2017).

The motivation of this work of research is to study these two mechanisms in a phenomenological manner. The following chapters will briefly introduce the size scale effects, the theory of strain gradient plasticity, the proposed interface modeling, and the implementation of all these into a finite element method (FEM) scheme. The complete discussion of these topics, however, are left for the appended papers.

# Small scale effects

The presence of particles in a matrix material makes the micro scale state of deformation heterogeneous. Experimental works have shown that a heterogeneous state of deformation means that size scale effects are introduced in the material. In this section, these experimental observations will be addressed very briefly, and then a brief introduction to available modeling approaches to study this phenomenon is given. The well-established strain gradient plasticity (SGP) approach, however, is explained separately in the next section, as it is the approach utilized in this work to study precipitation strengthening.

## Experimental observations

There are experimental evidence that proves the fact that in the presence of inhomogeneous plastic deformation, size effects appear, specifically in presence of gradients of plastic strain. These gradients can be a natural consequence of boundary conditions or even internal incompatibilities (like the mismatch between lattice structures of matrix material and second-phase particles). It is shown that the dislocation density is correlated to plastic strain and its gradient. If divided into two parts, the statistically stored density ($\rho_{\mathrm{SSD}}$) is related to the plastic strain, and the geometrically necessary density ($\rho_{\mathrm{GND}}$) is directly related to the gradient of plastic strain.

According to Fleck et al. (1994), the experimental observations of size scale effects can be categorized in three groups. *i) Size effects due to the microstructure.* This category concerns the effects of size and morphology of actual microstructures, such as size of inclusions and second-phase particles. The Hall-Petch effect (Hall (1951) and Petch (1953)) is a well-known example of this group. *ii) Locally sharp plastic gradients.* This group of experiments deal with severe local plastic deformations with sharp gradients, such as the deformation field around an indenter or a crack tip. The observations made by Oliver et al. (1985) that the decrease in indentation depth results in increased hardness measurement is an example of this group. *iii) Imposed macroscopic gradients.* This final

group covers the experiments with a macroscopically applied deformation gradient. A good example of this group is the work done by Fleck et al. (1994) where Cu wires with different diameters were tested in tension and torsion. The tension test results in a homogenous strain distribution throughout the wire thickness and hence showed negligible dependency on wire size, while the torsion test results in a gradient of strain (it varies from zero on the neutral axis to a finite strain on the surface) and hence showed effects of size scale.

# Modeling approaches

The conventional continuum treatment of plasticity will not capture effects of size scale, since its governing equations are devoid of any length scale parameter. Hence, there is a need for more complex approaches to study problems with size scale effects. Three of these approaches will be briefly introduced here.

**Molecular dynamics:** Molecular dynamics (MD) is the computer simulation of the physical movements of particles. In the most common version, the dynamic evolution equations of a system of interacting atoms and molecules are numerically solved over a fixed period of time. In this method, forces between the particles and their potential energies are often calculated using inter-atomic potentials or molecular mechanics force fields. The method was originally developed within the field of theoretical physics in the late 1950s, but is applied today mostly in chemical physics, materials science, and the modeling of bio-molecules (Mattis (1993), Alder and Wainwright (1959), Rahman (1964)).

There are also restrictions with this approach. MD simulations are computationally costly and generate cumulative errors in numerical integration. Even though the number of possible particles in each simulation has reached to the order of 100 million thanks to advancements in computational tools, it only encompasses a cube of material with 500 atoms in each direction, or equivalently, a cube with edge size of only 100 nm Schiotz and Jacobsen (2003). Another obstacle with MD is the extremely small time increments needed for the numerical integration. This is due to the fact that the time steps should be smaller than the shortest movement time scale of atoms. This problems can be partly solved by simulating atoms movements in very low temperatures. In order to get meaningful macroscopic strain levels for simulations on such a short time and low temperature, the loading should be applied on very high rates, namely in the order of $10^6$ - $10^8$ $s^{-1}$. So, MD simulations are normally carried out for extremely small specimens with extremely

high loading rates and extremely low temperatures, and hence they are only useful to give insight on the processes happening on the smallest possible scales, and in practice, they are used as an input to other approaches that operate on larger scales with less numerical constraints.

**Discrete dislocation dynamics:** In discrete dislocation dynamics (DD or DDD) approach, dislocation lines are represented explicitly. It treats the continuum as an elastic medium with embedded dislocation lines as elastic inclusions. The plastic behavior is then simulated by the collective evolution of a large number of interacting dislocations under an external loading. Properties of dislocations, such as line mobility and junction strength, can be derived from MD simulations. DD simulations are used both for evaluating the mechanical response of the material and analyzing the dislocation patterning (Schwarz and Tersoff (1996), Hirth et al. (1996), Zbib et al. (1998), Van der Giessen and Needleman (1995)).

The analytical description for stress and deformation state of an infinite, isotropic medium with an embedded elastic, linear dislocation is known for many types of dislocations. Hence, except in the core of dislocation that is a line singularity, this analytical solution is valid and accurate. To account for the effects of dislocation singularity, DD numerically solves a complementary field which, in addition to the analytical solution, results in equilibrium and compatibility in the medium. One restriction of the DD method is that by increasing plastic deformation, the number of dislocation line segments increases, and hence the computational cost increases gradually in each analysis. Nonetheless, DD approaches have been proved very useful in capturing microscale stress concentrations and failure processes which are not possible to be captured by other approaches.

**Crystal plasticity:** Crystal plasticity is based on the fact that crystals are mechanically anisotropic, and hence they cannot be modeled using conventional constitutive equations. This is due to the orientation dependence of the activation of the crystallographic deformation mechanisms (dislocations, twins, martensitic transformations). As a consequence of this, the macroscopic mechanical behavior of the material becomes orientation dependent (Roters et al. (2010), Uchic et al. (2004), Asaro (1983)).

The main application of crystal plasticity approach is to model the rotations of individual grains in a polycrystal, which will predict the evolution of texture, which, in turn, will result in the development of anisotropy in the solid. The constitutive models used in crystal plasticity are categorized as phenomenological and physics-based. In phe-

nomenological models, all slip systems of the crystal are taken into account and then the critical resolved shear stress in each of these systems are used as the state variables. In physics-based models, however, the dislocation density is used as the internal variable, since dislocations are the carriers of plastic strains. The density is then governed by physically-based evolution laws. Figure 7 shows the time and space domain of application of the aforementioned approaches.

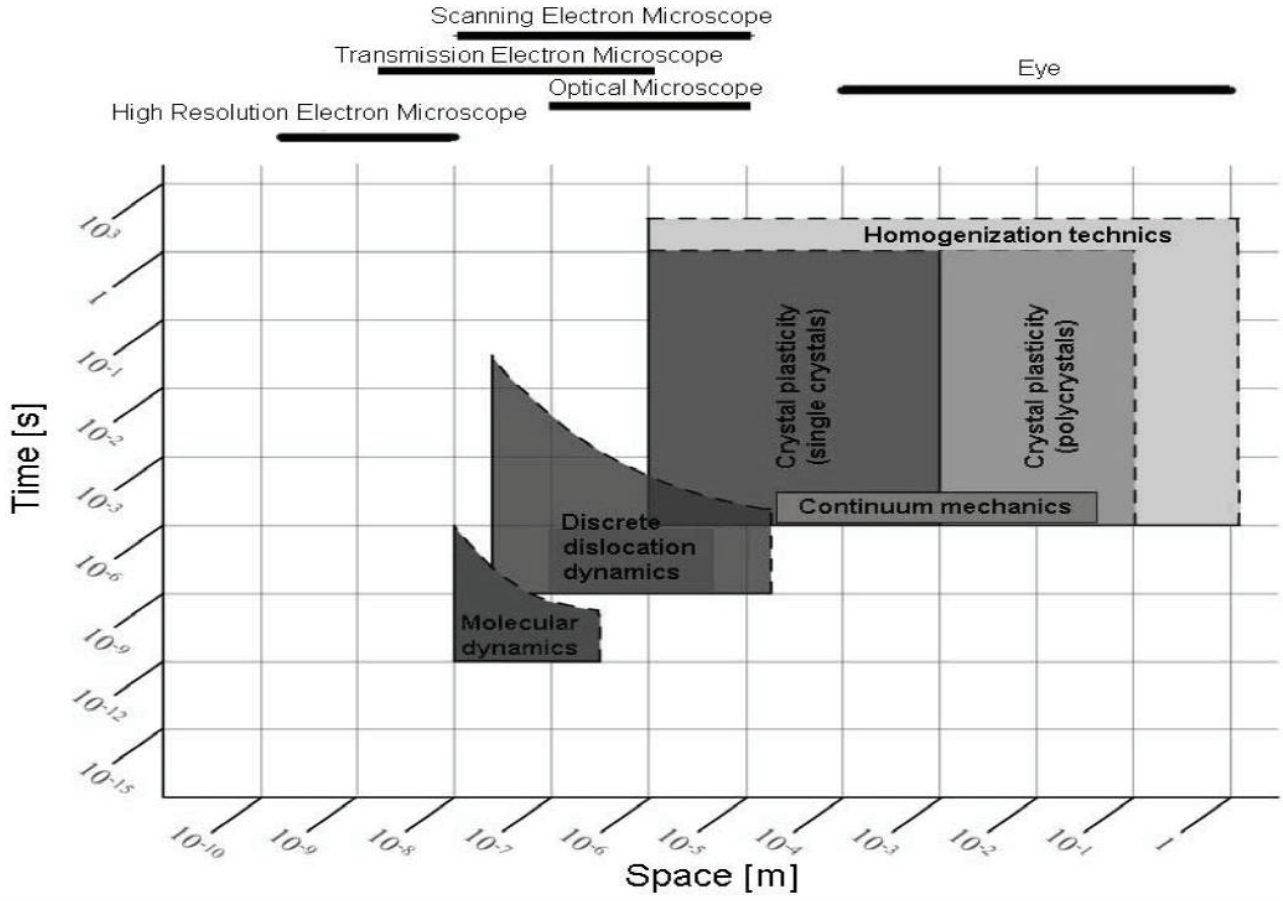


Figure 7: Typical size and physical time covered by three approaches introduced in this section. Figure taken from Fivel (2010).

# Strain gradient plasticity

As mentioned in the previous section, the approach used in this study to handle size scale effects is strain gradient plasticity (SGP). The main idea in SGP methods is that since strain is a dimensionless quantity, it cannot bring in any sense of size scale into the constitutive equations, and hence, the solution to this shortcoming is to include spatial gradients of strains to account for length scale effects. This is a similar fashion to rate dependent problems, where time derivatives bring in a sense of time scale. In principle, SGP models can be divided into two main categories: *lower order* theories, in which only the incremental constitutive relation is different from conventional plasticity, and *higher order* theories, which posses additional stress quantities and additional boundary conditions (Niordson and Hutchinson (2003)).

In all higher order theories, a measure of plastic strain and its spatial gradient enters the principle of virtual work (Fleck and Hutchinson (2001) and Gurtin (2000)). The work of this thesis is in the SGP framework introduced by Gudmundson (2004) and further developed in Fredriksson and Gudmundson (2005). For this isotropic, small strain theory, the internal virtual work is expressed as

$$\int_{\Omega} \left[\sigma_{ij}\delta\varepsilon_{ij} + (q_{ij} - s_{ij})\delta\varepsilon^{\mathrm{p}}_{ij} + m_{ijk}\delta\varepsilon^{\mathrm{p}}_{ij,k}\right] \mathrm{d}V = \int_{\partial\Omega} \left[T_i\delta u_i + M_{ij}\delta\varepsilon^{\mathrm{p}}_{ij}\right] \mathrm{d}S. \tag{2}$$

In the above equation, $\sigma_{ij}$ is the Cauchy stress and $s_{ij}$ is its deviatoric part. Moreover, there are a couple of additional stress quantities; $q_{ij}$ is the micro stress and $m_{ijk}$ is the moment stress, which are work conjugates to plastic strain tensor $\varepsilon^{\mathrm{p}}_{ij}$ and its spatial gradient tensor $\varepsilon^{\mathrm{p}}_{ij,k}$, respectively. Furthermore, $T_i = \sigma_{ij}n_j$ is the standard force traction and $M_{ij} = m_{ijk}n_k$ is the higher order moment traction. Finally, integration by parts of (2) and enforcing the arbitrariness of the virtual fields, give the strong form of equilibrium equations

$$\begin{aligned} &\sigma_{ij,j} = 0 \\ &m_{ijk,k} + s_{ij} - q_{ij} = 0. \end{aligned} \tag{3}$$

In absence of moment stresses, the second equation above reduces to $q_{ij} = s_{ij}$ and the conventional theory is recovered.

To make the formulation complete, constitutive equations have to be supplied. The Cauchy stress is governed by isotropic linear elasticity via Hooke's law

$$\sigma_{ij} = \frac{E}{1+\nu}\left(\varepsilon^{\mathrm{e}}_{ij} + \frac{\nu}{1-2\nu}\varepsilon^{\mathrm{e}}_{kk}\delta_{ij}\right). \tag{4}$$

where $E$ is Young's modulus and $\nu$ is Poisson's ratio. The constitutive equations for the non-standard stress tensors can be established by considering the fact that the rate of dissipation, which is the difference between the rate of internal work and the rate of change of free energy ($\psi$), must be non-negative at every point in the domain

$$(q_{ij} - \frac{\partial \psi}{\varepsilon^{\mathrm{p}}_{ij}})\dot{\varepsilon^{\mathrm{p}}_{ij}} + (m_{ijk} - \frac{\partial \psi}{\varepsilon^{\mathrm{p}}_{ij,k}})\dot{\varepsilon}^{\mathrm{p}}_{ij,k} \geq 0. \tag{5}$$

In all appended papers, it is assumed that $\psi$ is entirely associated with elastic strains. Hence, Eq. 5 is reduced to

$$q_{ij}\dot{\varepsilon^{\mathrm{p}}_{ij}} + m_{ijk}\dot{\varepsilon^{\mathrm{p}}_{ij,k}} \geq 0. \tag{6}$$

If $q_{ij}$ and $m_{ijk}$ are collinear with $\varepsilon^{\mathrm{p}}_{ij}$ and $\varepsilon^{\mathrm{p}}_{ij,k}$, respectively, Eq. 6 will be fulfilled (Gudmundson (2004)).

To construct effective measures of stress and strain, the rate of dissipation in Eq. 6 is rewritten as

$$q_{ij}\dot{\varepsilon^{\mathrm{p}}_{ij}} + m_{ijk}\dot{\varepsilon^{\mathrm{p}}_{ij,k}} = \Sigma \dot{E^{\mathrm{p}}}, \tag{7}$$

where $\Sigma$ and $E$ are effective measures of stress and strains, respectively. By an analogy to standard $J_2$-plasticity, the explicit form of these two parameters are suggested as

$$\Sigma = \sqrt{\frac{3}{2}\left(q_{ij}q_{ij} + \frac{m_{ijk}m_{ijk}}{\ell^2}\right)} \tag{8}$$

and

$$\dot{E^{\mathrm{p}}} = \sqrt{\frac{2}{3}\left(\dot{\varepsilon}^{\mathrm{p}}_{ij}\dot{\varepsilon}^{\mathrm{p}}_{ij} + \ell^2\dot{\varepsilon}^{\mathrm{p}}_{ij,k}\dot{\varepsilon}^{\mathrm{p}}_{ij,k}\right)}, \tag{9}$$

where the intrinsic material length scale parameter $\ell$ is introduced to make the dimensions consistent. This parameter is related to the characteristic length of the microstructure. There are analytical and experimental methods to measure the value of $\ell$, for example, see Gao and Huang (2003) and Abu Al-Rub and Voyiadjis (2004).

Taking the variation of Eq. 7 and using the definitions in Eq. 8 and 9, the constitutive equations for non-standard stress quantities are obtained as

$$q_{ij} = \frac{2}{3}\frac{\Sigma}{\dot{E^{\mathrm{p}}}}\dot{\varepsilon}^{\mathrm{p}}_{ij} \quad \text{and} \quad m_{ijk} = \frac{2}{3}\frac{\Sigma}{\dot{E^{\mathrm{p}}}}\ell^2\dot{\varepsilon}^{\mathrm{p}}_{ij,k}. \tag{10}$$

These constitutive equations can be rephrased in the inverted form as

$$\dot{\varepsilon}^{\mathrm{p}}_{ij} = \dot{\varepsilon}_0\frac{3q_{ij}}{2\Sigma}\ (\dot{E^{\mathrm{p}}}/\dot{\varepsilon}_0), \tag{11}$$

$$\dot{\varepsilon}^{\mathrm{p}}_{ij,k} = \dot{\varepsilon}_0 \frac{3m_{ijk}}{2\ell^2\Sigma} \, (\dot{E}^{\mathrm{p}}/\dot{\varepsilon}_0), \tag{12}$$

where $\dot{\varepsilon}_0$ is a reference strain rate. The $\dot{E}^{\mathrm{p}}/\dot{\varepsilon}_0$ term represents a viscoplastic response that depends on the effective stress and the inviscid flow stress $\sigma_{\mathrm{f}}$

$$\sigma_{\mathrm{f}} = \sigma_0 + H(E^{\mathrm{p}}) \tag{13}$$

where $\sigma_0$ is the yield stress for the matrix material, and $H$ represents hardening.

# Energetic interfaces

If internal interfaces are introduced in the material (e.g. the separating surface between matrix and second-phase particles), the SGP formulation given in previous section needs to be enhanced by extra terms. Hence, the virtual work functional is complemented by contributions from the work done on internal surfaces as

$$\int_{\Omega} \left[\sigma_{ij}\delta\varepsilon_{ij} + (q_{ij} - s_{ij})\delta\varepsilon^{\mathrm{p}}_{ij} + m_{ijk}\delta\varepsilon^{\mathrm{p}}_{ij,k}\right] \mathrm{d}V + \int_{\Gamma} \left[T_i\delta\bar{u}_i + M_{ij}\delta\bar{\varepsilon}^{\mathrm{p}}_{ij}\right] \mathrm{d}S = \int_{\partial\Omega} \left[T_i\delta u_i + M_{ij}\delta\varepsilon^{\mathrm{p}}_{ij}\right] \mathrm{d}S \tag{14}$$

in which $\bar{u}$ and $\bar{\varepsilon}$ are respectively some measures of displacement and plastic strain on the interface surface. In most interface models, $\bar{u}$ is chosen as the jump in displacement over the interface layer, while the choice for $\bar{\varepsilon}$ is more varied.

For barriers at which dislocations may pile up (such as the surface of second-phase particles), it is common to assume the internal interfaces are energetic, i.e. processes at the interface only change the energetic state and do not cause any dissipation (Aifantis et al. (2006); Borg and Fleck (2007)). Hence, an interface potential $\Psi_{\Gamma}$ can be considered from which the higher order tractions at the interface can be evaluated as

$$M_{ij} = \frac{\partial\Psi_{\Gamma}}{\partial\varepsilon^{\mathrm{p}}_{ij}}. \tag{15}$$

Here, $\epsilon(\varepsilon^{\mathrm{p}}_{ij})$ is defined as the norm of plastic strain at the interface, then

$$\frac{\partial\epsilon}{\partial\varepsilon^{\mathrm{p}}_{ij}} = \frac{\varepsilon^{\mathrm{p}}_{ij}}{\epsilon}. \tag{16}$$

Applying chain rule to Eq. 15 and inserting Eq. 16, the higher order traction components can be described as

$$M_{ij} = \frac{\partial\Psi_{\Gamma}}{\partial\epsilon}\frac{\partial\epsilon}{\partial\varepsilon^{\mathrm{p}}_{ij}} = \psi_{\Gamma}\frac{\varepsilon^{\mathrm{p}}_{ij}}{\epsilon} \tag{17}$$

in which $\psi_{\Gamma}$ is interface function.

Here, three interface models (including the model used in appended papers) are briefly introduced. The first model is by **Fredriksson and Gudmundson** (Fredriksson and

Gudmundson (2007)), in which the potential function has the general power law form of

$$\Psi_\Gamma = \frac{1}{N}\ell_\Gamma E(\frac{\sigma_y}{E})^{2-N}\epsilon_e^N. \tag{18}$$

Here, $\epsilon_e = \sqrt{\frac{2}{3}\varepsilon_{ij}^{pI}\varepsilon_{ij}^{pI}}$, and $\ell_\Gamma$ is a material length scale parameter different from the bulk length scale. If $\ell_\Gamma = 0$, the interface would allow dislocations to pass through freely, and if $\ell_\Gamma \to \infty$, the passage of dislocations is fully blocked and therefore $\varepsilon_{ij}^{pI} = 0$.

The second model is by **Dahlberg and Faleskog** (Dahlberg and Faleskog (2013)), which is based on the work of Fleck and Willis (2009). In this model, two effective measures for plastic strain at the interface are used as

$$\varepsilon^+ = \sqrt{\hat{\varepsilon}_{ij}\hat{\varepsilon}_{ij}} \quad \text{and} \quad \varepsilon^- = \sqrt{\check{\varepsilon}_{ij}\check{\varepsilon}_{ij}}, \tag{19}$$

in which $\hat{}$ and $\check{}$ stand for the difference and the average of each quantity at the interface, respectively. The interface energy function is given by

$$\psi_\Gamma(\varepsilon^\star) = \frac{G_0 L^\star\ \varepsilon^\star}{\left(1+\left(\frac{\varepsilon^\star}{\varepsilon_0}\right)^p\right)^{1/p}}\ , \tag{20}$$

where $p$ is the shape parameter, $\varepsilon_0$ is a reference strain, $G_0$ is the interface stiffness, $L^\star$ is the interface length scale, and the superscript $^\star$ should be substituted for either + or -.

The third interface model, which is proposed in the appended papers, is by **Asgharzadeh and Faleskog** (Asgharzadeh and Faleskog (2018)). In this model, it is assumed that one side of the interface is always occupied by elastic particles, and the effective strain is calculated by $\varepsilon_\Gamma = \sqrt{\varepsilon_{ij}^p\varepsilon_{ij}^p}$. An interface energy function that facilitates increase in both macroscopic yield strength and hardening is proposed as

$$\psi_\Gamma(\epsilon_\Gamma) = \alpha_0\ell\sigma_0 \cdot \left(1+\alpha_1\frac{\varepsilon_\Gamma G_m}{\alpha_0\sigma_0}\right)\ . \tag{21}$$

Here, the shear modulus of the matrix material $G_m$ is introduced for dimensional reasons. This function contains two key parameters $\alpha_0$ and $\alpha_1$, and it should be interpreted as follows: the first term defines the strength of the interface which results in the increase in yield stress of the material, while the second term affects the increase in plastic work hardening of the material. This model is described in more details in the first appended paper.

# Finite element implementation

The theories briefly introduced in the previous sections were discretized and implemented into a finite element method (FEM) framework. The work done for plane strain in Dahlberg and Faleskog (2013) has been used as the basis to develop the formulation further into axi-symmetric (first appended paper) and general 3D conditions (the rest of appended papers). In the current higher order framework, in addition to displacement as conventional degrees of freedom (DOF), plastic strains are also considered as DOF. Hence, in the case of axi-symmetry, the DOF components are

$$\mathbf{d}_{\mathrm{u}}^{\mathrm{T}} = [u_r \quad u_z], \quad \mathbf{d}_{\mathrm{p}}^{\mathrm{T}} = [\varepsilon_{rr}^{\mathrm{p}} \; \varepsilon_{zz}^{\mathrm{p}} \; \gamma_{rz}^{\mathrm{p}}], \tag{22}$$

and the DOF components in 3D formulations are

$$\mathbf{d}_{\mathrm{u}}^{\mathrm{T}} = [u_x \quad u_y \quad u_z], \quad \mathbf{d}_{\mathrm{p}}^{\mathrm{T}} = [\epsilon_{xx}^{\mathrm{p}} \quad \epsilon_{yy}^{\mathrm{p}} \quad \gamma_{xy}^{\mathrm{p}} \quad \gamma_{xz}^{\mathrm{p}} \quad \gamma_{yz}^{\mathrm{p}}]. \tag{23}$$

In both equations above, plastic incompressibility is assumed, i.e. $\varepsilon_{\phi\phi}^{\mathrm{p}} = -(\varepsilon_{rr}^{\mathrm{p}} + \varepsilon_{zz}^{\mathrm{p}})$ and $\varepsilon_{zz}^{\mathrm{p}} = -(\varepsilon_{xx}^{\mathrm{p}} + \varepsilon_{yy}^{\mathrm{p}})$, respectively.

Displacements and plastic strains at any arbitrary point within elements can be found by using shape functions and nodal values as

$$\begin{bmatrix} \boldsymbol{u} \\ \boldsymbol{\varepsilon}^{\mathrm{p}} \end{bmatrix} = \begin{bmatrix} \mathbb{N}_{\mathrm{u}} & \mathbb{O} \\ \mathbb{O} & \mathbb{N}_{\mathrm{p}} \end{bmatrix} \begin{bmatrix} \boldsymbol{d}_{\mathrm{u}} \\ \boldsymbol{d}_{\mathrm{p}} \end{bmatrix}, \tag{24}$$

in which $\mathbb{N}_{\mathrm{u}}$ is the shape function matrix for displacements DOF, $\mathbb{N}_{\mathrm{p}}$ is the shape function matrix for plastic strains DOF, and $\mathbb{O}$ is the zero matrix of appropriate size. The choice of element type will decide the components of $\mathbb{N}_{\mathrm{u}}$ and $\mathbb{N}_{\mathrm{p}}$ matrices.

Figures 8 and 9 show the type of elements developed and employed in the appended papers. In the axi-symmetric case, the bulk is modeled by 8-node serendipity element and the interface by quadratic line elements, while in the 3D case, the bulk is modeled by 10-node quadratic elements and the interface by quadratic triangle elements. It should be noted that nodes with filled circles posses both displacement and plastic strain DOF, while nodes with hollow circles posses only displacement DOF. So, $\mathbb{N}_{\mathrm{u}}$ is quadratic while

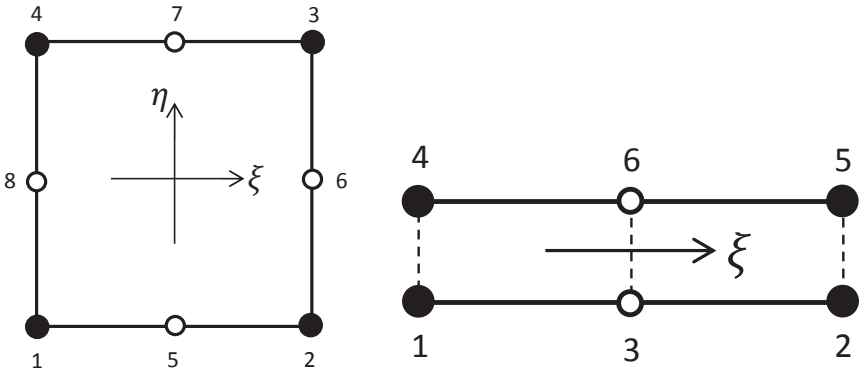


Figure 8: Elements used in axi-symmetric case.

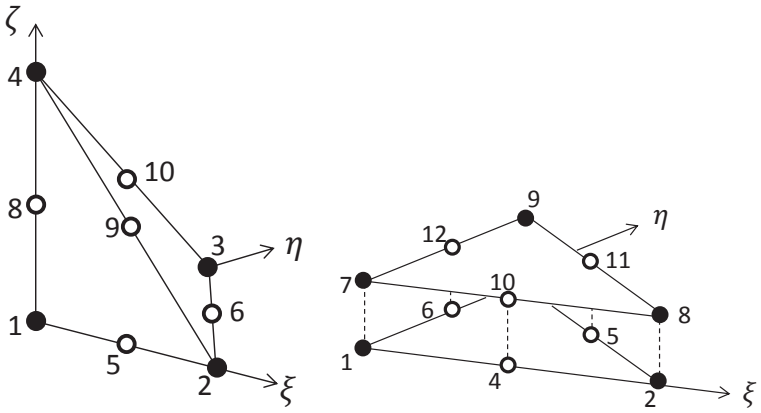


Figure 9: Elements used in 3D case.

$\mathbb{N}_p$ is linear. The geometry is also interpolated using the quadratic shape functions, and for numerical convenience, the quadratic Jacobian matrix is used in spatial description of plastic strain DOF, because if two different geometry interpolations are used, the Gauss points will not coincide. Figure 10 shows number of Gauss points used in this work.

| | **Bulk Element** | **Interface Element** |
|---|---|---|
| Axisymmetric | 4 | 2 |
| Three Dimensional | 4 | 3 |

Figure 10: Number of Gauss points used in each element.

Initialize solution: $t = 0$, $f_t = 1.0$, $\Delta t = \Delta t_0$, $\boldsymbol{d}^{(t)} = \mathbf{0}$ and $\boldsymbol{E}^{\mathrm{p}} = \mathbf{0}$
**while** solution is not done **do**
  Initialize load step: $e = 1.0$, $k = 0$
  $\Delta \boldsymbol{d}_{\mathrm{u}}^{k} = \mathbf{0}$, $\Delta \boldsymbol{d}_{\mathrm{p}}^{k} = f_t \Delta \boldsymbol{d}_{\mathrm{p}}^{(t)}$ and $\boldsymbol{d}^{k} = \boldsymbol{d}^{(t)} + \Delta \boldsymbol{d}^{k}$
  **while** $e >$ `tol` **and** $k <$ `maxiter` **do**
    $k \leftarrow k + 1$, $\mathbb{K}_{\mathrm{tan}} = \mathbb{O}$, $\boldsymbol{f}_{\mathrm{int}} = \mathbf{0}$, $\boldsymbol{E}^{\mathrm{trial}} = \mathbf{0}$
    **for** all elements **do**
      % Quantities in this loop refer to each element only
      $\boldsymbol{\epsilon} = \mathbb{B}\boldsymbol{d}^{(t)}$, $\Delta\boldsymbol{\epsilon} = \mathbb{B}\left(\boldsymbol{d}^{k} - \boldsymbol{d}^{(t)}\right)$, $\mathbb{K} = \mathbb{O}$, $\boldsymbol{f} = \mathbf{0}$
      **for** all Gauss points **do**
        % Quantities in this loop refer to each Gauss point only
        Calculate $\Delta E^{\mathrm{p}}$ from $\Delta\boldsymbol{\epsilon}$ and update $\sigma_{\mathrm{f}}(E^{\mathrm{p}} + \Delta E^{\mathrm{p}})$
        Solve nonlinear equation for $\Sigma$ and update $\boldsymbol{s}$
        Calculate the algorithmic $\mathbb{D}$ from the updated state
        $\mathbb{K} \leftarrow \mathbb{K} + \mathbb{B}^{\mathrm{T}}\mathbb{D}\mathbb{B}Jw$ and $\boldsymbol{f} \leftarrow \boldsymbol{f} + \mathbb{B}^{\mathrm{T}}\boldsymbol{s}Jw$
      **end for**
      $\boldsymbol{E}^{\mathrm{trial}} = \boldsymbol{E}^{\mathrm{p}} + \Delta\boldsymbol{E}^{\mathrm{p}}$
      Assemble: $\mathbb{K}_{\mathrm{tan}} \leftarrow \mathbb{K}_{\mathrm{tan}} + \mathbb{K}$ and $\boldsymbol{f}_{\mathrm{int}} \leftarrow \boldsymbol{f}_{\mathrm{int}} + \boldsymbol{f}$
    **end for**
    Apply boundary conditions and Lagrange multiplier equations
    Solve $\mathbb{K}_{\mathrm{tan}}\Delta\boldsymbol{d}^{k} = \boldsymbol{f}_{\mathrm{ext}} - \boldsymbol{f}_{\mathrm{int}}$ for $\Delta\boldsymbol{d}^{k}$
    $\boldsymbol{d}^{k} \leftarrow \boldsymbol{d}^{k} + \Delta\boldsymbol{d}^{k}$ and calculate $e = \|\Delta\boldsymbol{d}^{k}\|/\|\boldsymbol{d}^{k} - \boldsymbol{d}^{(t)}\|$
  **end while**
  **if** load step converged **then**
    Update $\Delta\boldsymbol{d}^{(t+\Delta t)} = \boldsymbol{d}^{k} - \boldsymbol{d}^{(t)}$, $\boldsymbol{d}^{(t+\Delta t)} = \boldsymbol{d}^{k}$ and $\boldsymbol{E}^{\mathrm{p}} = \boldsymbol{E}^{\mathrm{trial}}$
    $t \leftarrow t + \Delta t$
    Calculate new $f_t$, $\Delta t \leftarrow f_t \Delta t$ and check for end of solution
  **else**
    $\Delta t \leftarrow \Delta t/2$, check for stop condition
  **end if**
**end while**

Figure 11: Backward-Euler algorithm. Figure taken from Dahlberg (2011).

The implementation is done in a fully implicit backward-Euler scheme into an in-house Fortran program, with the details of the algorithm shown in figure 11. Intel PARDISO is utilized as the parallel direct sparse solver, which is a robust and efficient solver with great memory handling features (see Schenk and Gartner (2004) and Gould et al. (2007)). In addition, a set of programs in Fortran and Matlab are used for pre- and post-processing, and Ansys is used in the meshing of 3D geometries. The analyses are executed in parallel form by use of OpenMP application programming interface on a computer cluster with 8 nodes, each composed of 8 threads.

# Problem definition

Figure 12 depicts the schematic of a continuum with a distribution of small particles. The average radius is shown as $r_p$, which is found to be in the range of a few to several hundreds of nanometers. Two other important parameters for the strengthening are also mentioned in the figure, namely the average distance between particles $L_p$, and the length scale characteristic of the matrix material $\ell$. The plastic deformation processes –which lead to strengthening– occur at the scale of $\ell$. Hence, the effect of length parameters characterizing the micro-structure, i.e. $L_p$ and $r_p$, should also be related to $\ell$.

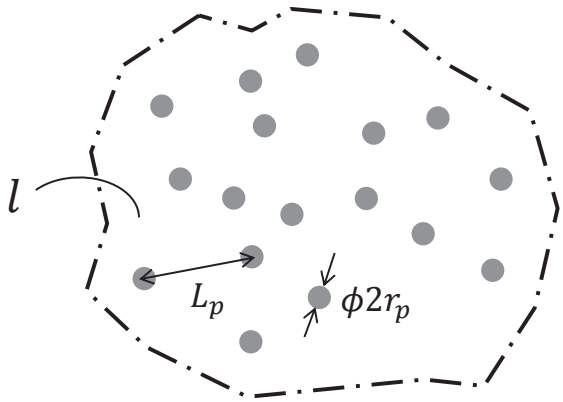


Figure 12: Schematic of a micro-structure containing a distribution of particles.

In this work, evaluating the increase in yield strength (strengthening) due to presence of particles is the objective. To make a numerical study possible, some approximations are made. First of all, both matrix and particle materials are considered to be isotropic. Secondly, particles are assumed to deform only elastically. And thirdly, a globally periodic distribution of particles is considered. This means, even if the distribution is locally random, the global distribution can be reproduced by copying a unit cell in three dimensions. Four of such unit cells are then chosen to build the microstructure. Each of the appended papers is based on one of these microstructures, see next section, *Summary of appended papers*.

The microstructures are modeled in the FEM framework implemented from the higher order SGP and the energetic interface theories introduced in previous sections. The purpose of using SGP is to bring in a sense of length scale, and the purpose of using the energetic interface is to –qualitatively– mimic the pile up of dislocations on particles surfaces. Finally, the models are subjected to uniaxial tension (and simple shear for Paper D). Since the components of each model are isotropic, the direction of loading does not affect the behavior. A summary of obtained results are presented in the upcoming section *Key results*.

# Modelling

The theoretical framework and numerical implementation briefly introduced in previous sections are applied to four different micromechanical models to study the precipitation strengthening, which are appended as four independent papers to this text. Here, a summary of these papers is given.

**Paper A:** *Strengthening effects of particle-matrix interaction analyzed by an axi-symmetric model based on strain gradient plasticity*

The main purpose of the first paper is to introduce and elaborate on the new interface model proposed by the authors, which is used in papers B-D as well. In order to make it numerically affordable to have a vast range of parametric study, the micromechanical model is chosen as simple as possible. Hence, an axi-symmetric model including one particle is used (Fig. 13). The effect of different parameters on the macroscopic response of the RVE is analyzed, including, but not limited to, particle size, material length scale, shear modulus mismatch between particle and matrix, and interface strength. It is concluded that the strengthening observed in this model can be formulated in a closed-form equation.

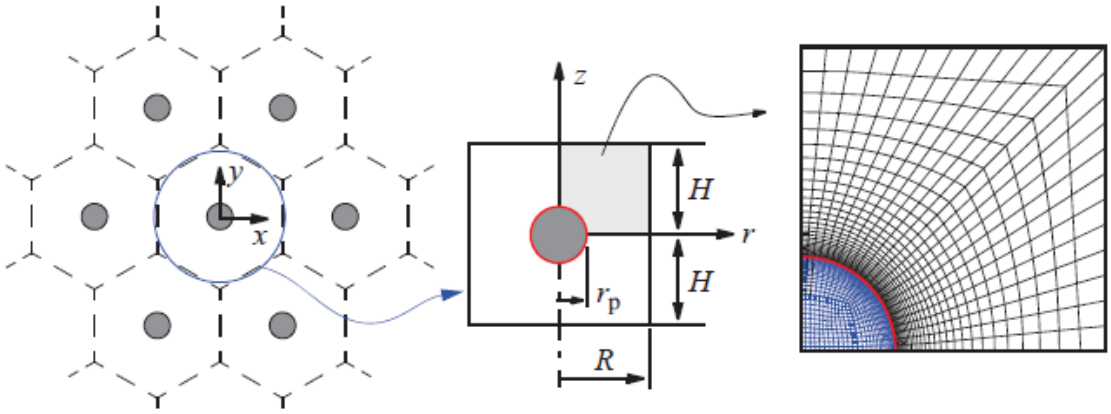


Figure 13: The axi-symmetric model used in paper A.

**Paper B:** *A model for precipitation strengthening accounting for variations of particle size and spacing based on strain gradient plasticity in 3D*

This paper is written with the main purpose of expanding the 2D framework introduced in paper A to a 3D space. The micromechanical model is composed of an RVE accommodating for eight different particles, as can be seen in Fig. 14. This RVE is the result of the assumption of periodic distribution for particles. This 3D model makes it possible to study the effects of particle size distribution, since it includes more than one particle. In this paper, a set of parametric study is performed to complement what is done in paper A, including, for example, the effects of coefficient of variation of particle size distribution on the strengthening of the material. It is shown that the closed-form formulation introduced in paper A is applicable to these 3D results, too.

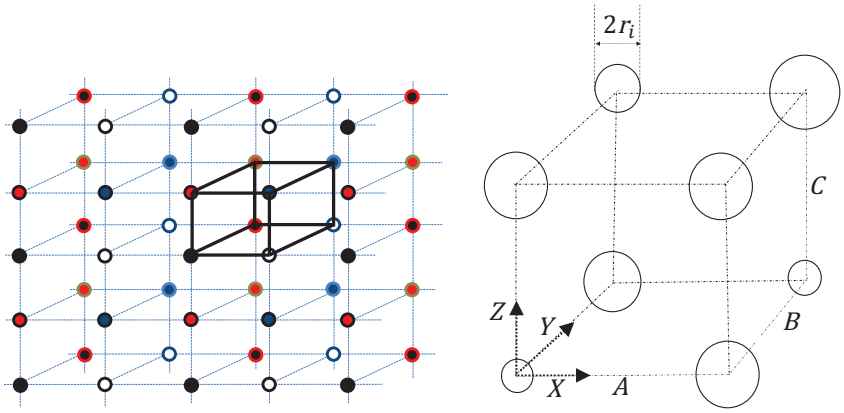


Figure 14: The 3D ordered model used in paper B.

**Paper C:** *A 3D model for the analysis of plastic flow properties of randomly-distributed particles*

For the sake of the generality of the model, a completely random distribution of particles is considered in paper C, resulting in the RVE depicted in Fig. 15. The new dimension this model brings in is the possibility to have a realistic particle spacing distribution (different distance between different particles). As the final paper on the Orowan phase of precipitation strengthening, a complementary set of parametric studies are carried out. The proposed closed-form formulation is approved to be applicable in the general 3D space, and the numerical results are compared with experimental data available in literature, for two main categories of particle-hardened materials, namely age-hardened alloys and metal matrix composites (MMCs).

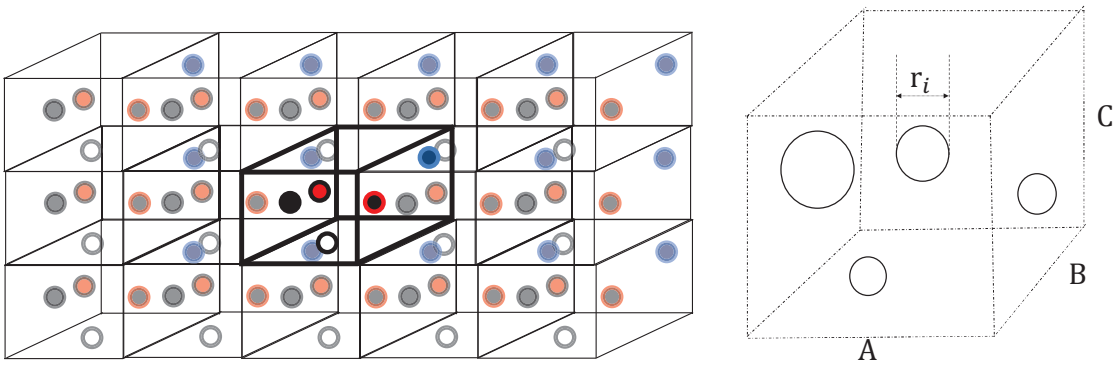


Figure 15: The 3D random model used in paper C.

**Paper D:** *A shearing/looping transition model for precipitation strengthening*

In order to cover the whole range of precipitation strengthening, an RVE with an embedded discrete slip plane is introduced in paper D, as can be seen in Fig. 16. The idea here is that when the stress in the microstructure reaches to a specific level, the sliding feature gets triggered and hence it will simulate the shearing of the particle. Since this model is constructed based on what is done in papers A-C, in case that the shearing mechanism does not get engaged, it still has the capability to mimic the Orowan response. Effects of different parameters on the precipitation strengthening in the shearing mode are studied, and by use of a Taylor homogenization scheme, consequences of having a size distribution of particles is demonstrated.

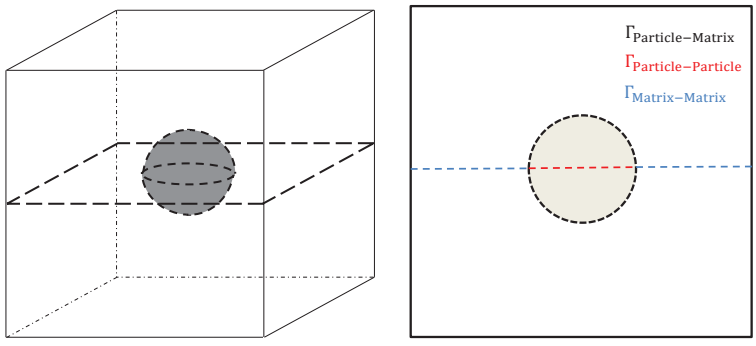


Figure 16: The 3D shearing model used in paper D.

# Key results

Here, the most important observations made in the appended papers are briefly presented. The macroscopic stress-strain curves are evaluated by volume averaging of strain and stress fields within each RVE. Two key parameters controlling macroscopic behavior are interface strength $\alpha_0$ and particle spacing $L_\mathrm{p}$ (normalized by material length scale $\ell$). Figure 17 shows such effects. Strengthening increases as $\alpha_0$ gets bigger (particle becomes more incoherent) or $L_\mathrm{p}$ gets smaller (the distance between particles shrink).

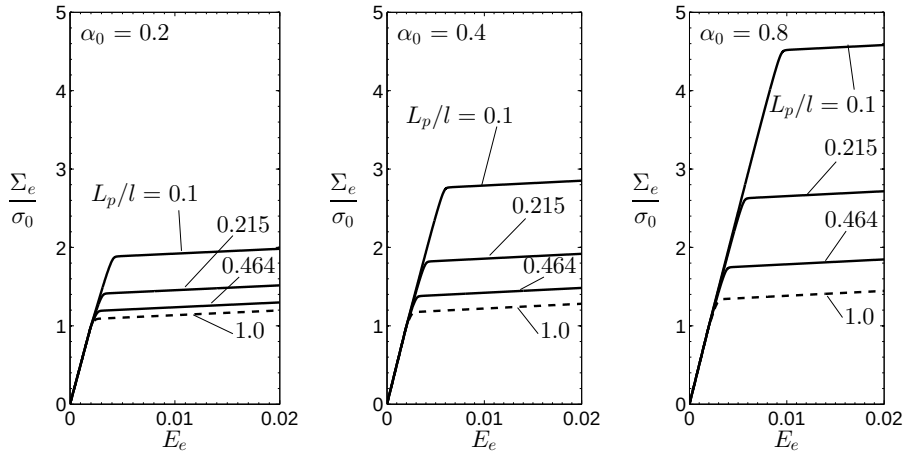


Figure 17: Effects of $\alpha_0$ and $L_\mathrm{p}$ on macroscopic stress-strain curves.

Another determining parameter is the volume fraction of particles $f$. The results obtained from the appended papers (including Figure 18) show that the dependency of strengthening on volume fraction of particles follows a power law. The mismatch between shear moduli of particle and matrix materials are also found to influence the strengthening. Figure 19 shows such an influence. The results from analyses carried out in appended papers reveal how each model's parameter affects the macroscopic response and hence the strengthening.

Moreover, it has been shown that all these effects can be compacted into a closed-form

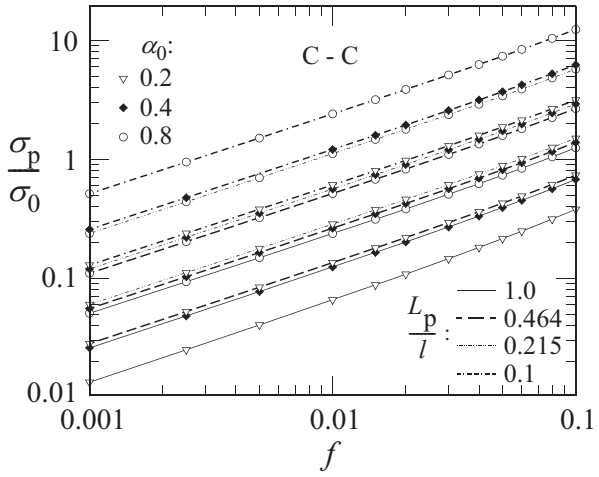


Figure 18: The increase in yield strength as a function of particles volume fraction.

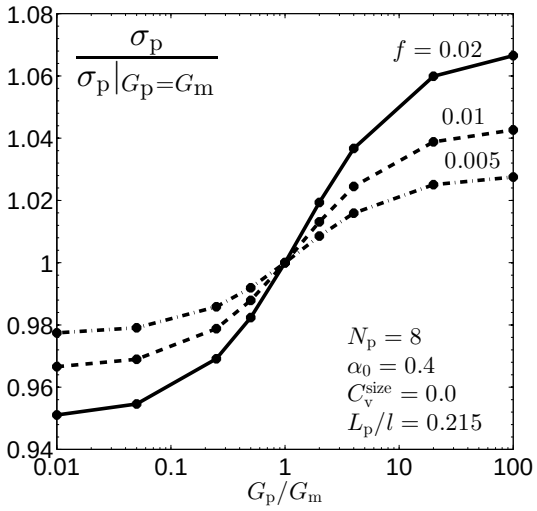


Figure 19: The increase in yield onset as a function of particle shear modulus.

function as

$$\frac{\sigma_p}{\sigma_0} = F_\sigma \left( \alpha_0, \frac{L_p}{\ell}, f, \frac{G_p}{G_m} \right). \tag{25}$$

The introduction of this formula has made it numerically convenient to compare the results of this study with experiments. Figure 20 shows one example of comparing numerical results of this work versus experimental results for magnesium reinforced with alumina particles $Mg - Al_2O_3$ (data from Hassan and Gupta (2004); Wong et al. (2005); Wong and Gupta (2007)). And finally, the model with an embedded slip plane which is used in Paper D has made it possible to include the shearing mechanism in the covered spectrum

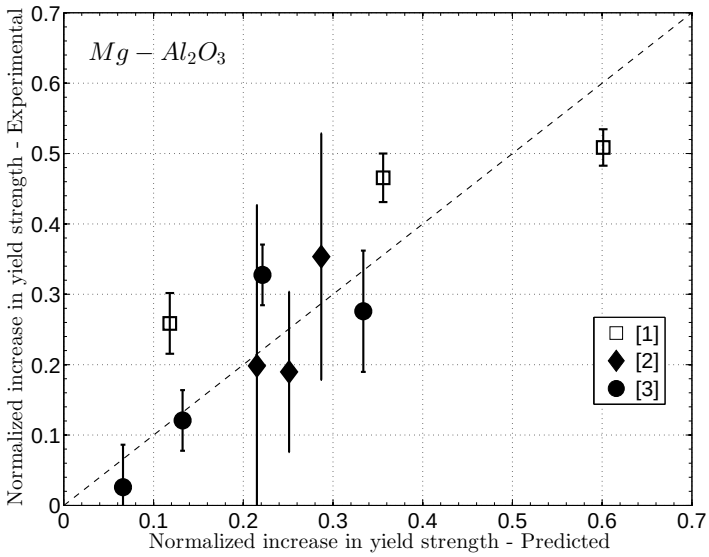


Figure 20: Comparison between predicted and measured strengths for $Mg - Al_2O_3$.

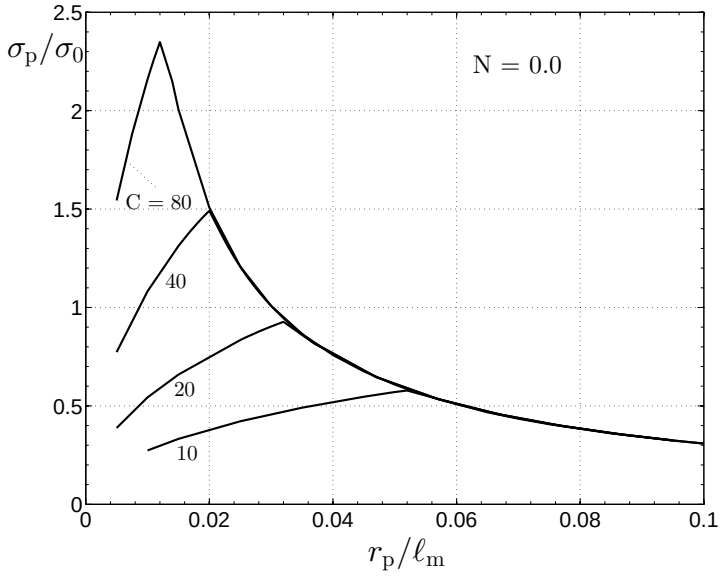


Figure 21: The transition from shearing to Orowan mechanisms.

of this print. Figure 21 shows the transition between shearing and Orowan mechanisms.

# Concluding remarks

Numerical study of precipitation strengthening has been set as the goal of this work of research. Different 2D- and 3D-micromechanical models have been proposed to fulfill this matter. Comprehensive parametric studies have been carried out, with the results being presented in the appended papers. To account for the effects of microstructure size scale, an SGP theory has been used. The numerical results have been compared with available experiments, and they have shown agreement both qualitatively and quantitatively. In the Orowan regime, decreasing particle size leads to more strengthening, while in the shearing regime, smaller particle sizes mean less strengthening. Furthermore, to bring in the effects of particle coherency, a new interface formulation has been introduced.

In addition, effects of having distributions for particles size and spacing have been studied. It has been shown that, for the Orowan regime, more homogenous size and more heterogeneous spacing distributions will result in peak strengthening performance. Similar findings have been observed for the shearing regime. Moreover, the increase in yield stress in the Orowan regime has been found to follow a closed-form formulation. Based on this formulation, effects of all parameters on the strengthening can be compacted in only two key parameters; the volume fraction of particles, and their surface area per unit volume of material. For a fixed volume fraction, the configuration with more surface area will be stronger, i.e. having more smaller particles is better than having a large one.

# Bibliography


Abu Al-Rub, R. K. and Voyiadjis, G. Z. (2004). Analytical and experimental determination of the material intrinsic length scale of strain gradient plasticity theory from micro- and nano-indentation experiments. *International Journal of Plasticity*, 20(6):1139–1182.

Aifantis, K. E., Soer, W. A., De Hosson, J. T. M., and Willis, J. R. (2006). Interfaces within strain graident plasticity: Theory and experiments. *acta*, 54:5077–5085.

Alder, B. J. and Wainwright, T. E. (1959). Studies in molecular dynamics. i. general method. *The Journal of chemical physics*, 31(2):459–466.

Asaro, R. J. (1983). Crystal plasticity. *Journal of Applied Mechanics, Transactions ASME*, 50(4):921–934.

Asgharzadeh, M. and Faleskog, J. (2018). Strengthening effects of particle-matrix interaction analyzed by an axi-symmetric model based on strain gradient plasticity. Submitted for publication.

Borg, U. and Fleck, N. A. (2007). Strain gradient effects in surface roughening. *msmse*, 15:S1–S12.

D Callister, W. (2018). Materials science and engineering : an introduction / william d. callister. *SERBIULA (sistema Librum 2.0)*.

Dahlberg, C. F. O. (2011). *On the Role of Interfaces in Small Scale Plasticity*. PhD thesis, KTH, Solid Mechanics (Div.). QC 20111118.

Dahlberg, C. F. O. and Faleskog, J. (2013). An improved strain gradient plasticity formulation with energetic interfaces: theory and a fully implicit finite element formulation. *Computational Mechanics*, 51:641–659.

Fivel, M. (2010). *Discrete Dislocation Dynamics: Principles and Recent Applications*, chapter 2, pages 17–36. John Wiley and Sons, Ltd.

Fleck, N. A. and Hutchinson, J. W. (2001). A reformulation of strain gradient plasticity. *Journal of the Mechanics and Physics of Solids*, 49:2245–2271.

Fleck, N. A., Muller, G. M., Ashby, M. F., and Hutchinson, J. W. (1994). Strain gradient plasticity - theory and experiment. *Acta Metallurgica Et Materialia*, 42(2):475–487.

Fleck, N. A. and Willis, J. R. (2009). A mathematical basis for strain-gradient plasticity theory. part ii: Tensorial plastic multiplier. *Journal of the Mechanics and Physics of Solids*, 57:1045–1057.

Fredriksson, P. and Gudmundson, P. (2005). Size-dependent yield strength of thin films. *International Journal of Plasticity*, 21(9):1834–1854.

Fredriksson, P. and Gudmundson, P. (2007). Modelling of the interface between a thin film and a substrate within a strain gradient plasticity framework. *Journal of the Mechanics and Physics of Solids*, 55(5):939–955.

Gao, H. and Huang, Y. (2003). Geometrically necessary dislocation and size-dependent plasticity. *Scripta Materialia*, 48(2):113–118.

Gould, N. I. M., Scott, J. A., and Hu, Y. (2007). A numerical evaluation of sparse direct solvers for the solution of large sparse symmetric linear systems of equations. *ACM Transactions on Mathematical Software*, 33(2).

Gudmundson, P. (2004). A unified treatment of strain gradient plasticity. *Journal of the Mechanics and Physics of Solids*, 52:1379–1406.

Gurtin, M. E. (2000). On the plasticity of single crystals: free energy, microforces, plastic-strain gradients. *Journal of the Mechanics and Physics of Solids*, 48(5):989 – 1036.

Hall, E. O. (1951). The Deformation and Ageing of Mild Steel: III Discussion of Results. *Proceedings of the Physical Society. Section B*, 64(9):747–753.

Hassan, S. F. and Gupta, M. (2004). Development of high performance magnesium nanocomposites using solidification processing route. *Materials Science and Technology*, 20:1383–1388.

Hirth, J. P., Rhee, M., and Zbib, H. (1996). Modeling of deformation by a 3d simulation of multiple, curved dislocations. *Journal of Computer-Aided Materials Design*, 3(1-3):164–166.

Jonsson, S. (2007). *Mechanical Properties of Metals and Dislocation Theory from an Engineer's Perspective*. Department of Materials Science and Engineering, Royal Institute of Technology.

Mattis, D. C. (1993). *The Many-Body Problem*. WORLD SCIENTIFIC.

McNamara, D. (2009). *How do eclogites deform in subduction and collision zones? An Alpine study*. PhD thesis, National University of Ireland, Galway — NUI Galway.

Niordson, C. F. and Hutchinson, J. W. (2003). On lower order strain gradient plasticity theories. *European Journal of Mechanics, A/Solids*, 22:771–778.

Oliver, W. C., Hutchings, R., and Pethica, J. B. (1985). Measurement of hardness at indentation depths as low as 20 nanometres. In *ASTM Special Technical Publication*, pages 90–108.

Petch, N. J. (1953). The cleavage strength of polycrystals. *The Journal of the Iron and Steel Institute*, 174:25–28.

Rahman, A. (1964). Correlations in the motion of atoms in liquid argon. *Physical Review*, 136(2A):A405–A411.

Rollett, A., Rohrer, G., and Humphreys, J. (2017). *Recrystallization and Related Annealing Phenomena*. Elsevier Science.

Roters, F., Eisenlohr, P., Hantcherli, L., Tjahjanto, D. D., Bieler, T. R., and Raabe, D. (2010). Overview of constitutive laws, kinematics, homogenization and multiscale methods in crystal plasticity finite-element modeling: Theory, experiments, applications. *Acta Materialia*, 58(4):1152–1211.

Schenk, O. and Gartner, K. (2004). Solving unsymmetric sparse systems of linear equations with pardiso. *Future Generation Computer Systems*, 20(3):475–487.

Schiotz, J. and Jacobsen, K. W. (2003). A maximum in the strength of nanocrystalline copper. *Science*, 301(5638):1357–1359.

Schwarz, K. W. and Tersoff, J. (1996). Interaction of threading and misfit dislocations in a strained epitaxial layer. *Applied Physics Letters*, 69(9):1220–1222.

Uchic, M. D., Dimiduk, D. M., Florando, J. N., and Nix, W. D. (2004). Sample dimensions influence strength and crystal plasticity. *Science*, 305(5686):986–989.

Van der Giessen, E. and Needleman, A. (1995). Discrete dislocation plasticity: A simple planar model. *Modelling and Simulation in Materials Science and Engineering*, 3(5):689–735.

Wong, W. L. E. and Gupta, M. (2007). Improving overall mechanical performance of magnesium using nano-alumina reinforcement and energy efficient microwave assisted processing route. *Advanced Engineering Materials*, 9:902–909.

Wong, W. L. E., Karthik, S., and Gupta, M. (2005). Development of hybrid mg/al 2o 3 composites with improved properties using microwave assisted rapid sintering route. *Journal of Materials Science*, 40:3395–3402.

Zbib, H. M., Rhee, M., and Hirth, J. P. (1998). On plastic deformation and the dynamics of 3d dislocations. *International Journal of Mechanical Sciences*, 40(2-3):113–127.